Vol. 42, No. 4 (2020) 679-691, DOI: 10.24874/ti.924.07.20.11

Tribology in Industry

www.tribology.rs

RESEARCH

HfN Coating of ASSAB 17 Steel by PVD Method and its Effects on 6063-T5 Aluminum Alloy Turning

J. Ortíz[a], J. Caicedo[b], J. Navarro-Devia[c], J. Martinez[a], W. Aperador[a,*]

[a] *School of Engineering, Universidad Militar Nueva Granada, Bogotá, Colombia,*
[b] *Tribology, Polymers, Powder Metallurgy and Processing of Recycled Solids Research Group, Universidad del Valle, Cali, Colombia,*
[c] *School of Engineering and Built Environment, Griffith University, Gold Coast, Queensland, Australia.*

Keywords:

Hafnium nitride
Aluminum
Cutting tool
Wear
Coatings

* Corresponding author:

Author W. Aperador
E-mail:
william.aperador@unimilitar.edu.co

Received: 7 July 2020
Revised: 16 August 2020
Accepted: 21 November 2020

A B S T R A C T

The industrial tool performance inspires the study of the machining of several materials with low production downtime. Aluminum is well-known for its high strength-to-weight ratio when compare both plastic and raft, thus making it advantageous for aerospace, construction and transport applications. However, aluminum machining damages the cutting tool with diverse wear mechanisms (adhesion, abrasion), thus suggesting a need for a new coating material. Previous studies show a high performance in abrasion resistance of Hafnium nitride [HfN] coated tools in turning of AISI1020 steel. This article evaluates the performance of [HfN] coated and uncoated burins (ASSAB 17) through roughing of Aluminum profiles by temperature sensing at the tool/material interface, workpiece roughness measurement and inspection of the cutting tool wear. Scanning electron microscopy and confocal microscopy were used to identify tool wear. A digital temperature sensing device displaying infrared long-wavelength was designed to examine the temperature due to its correlation on the tool wear. A significant improvement during aluminum roughing was observed with the use of [HfN] coatings, due to increase of the wear resistance of the ASSAB 17 burin, thus improving the surface finish.

1. INTRODUCTION

The efficiency, performance and cost reduction demanded by the industries that manufacture different mechanical components such as cylinders, axles, bushings, among others, inspires the continuous research for a versatile cutting material to machine different parts that has a high useful life reducing the inherent costs of maintenance and tool change [1-2]. However, within the most used machined materials, the properties of Aluminum limit the selection of cutting tools presenting a low production cost. In addition, it requires a prolonged performance to reduce the manufacturing time and the acquisition costs of the cutting tools lot [3].

Aluminum is one of the most used materials in the manufacture of mechanical components for applications in the naval industry, aerospace, construction, and transport, and it is still one of the most studied and employed materials in diverse manufacturing applications, even due the recent use of other materials [4-5]. It is well known the need for various turning cycles when machining aluminum as well as occurrence of adhesion and abrasion wear mechanisms of cutting tools [4-7]. The adhesion in the burins produces geometrical irregularities in the tip (e.g., re-growth of the edge) caused by the melting temperature of the Aluminum at the tool/material interface [8]. These geometric irregularities vary the dimensions of the cutting tool thus decreasing the quality of the surface finish, as abrasion mainly due to the impurities of the facing results in the displacement of materials and therefore, the generation of new particles or scratches which modifies the formation of chips and cutting forces, negatively altering the surface finish of the part [9-12].

Cutting tools used in several machining processes which are controlled by numerical control (NC) code, continuously operating under lubrication-free conditions (*dry machining*) [12-13]. As consequence the cutting tool lifetime is shortened. Therefore, the industry reports a constant need to increase both the life of the cutting tool and the precision of surface finish. The use of these hard coatings promotes an increase in machining productivity and most cases also decreases the need for lubricants [12-14].

Nowadays, hard coatings are more frequently used ceramic inserts due to these increase the wear resistance to various mechanisms such as abrasive and chemical wear [14-16]. Thin films reduce edge regrowth, thermal cracking and chipping in the cut, thus generating both a better production performance and significantly reduced machinery standstill [16-17]. Nevertheless, the cost of these inserts is much higher than conventional high-speed steel cutting tools [18-21].

Most of the cuttings tools in the market currently implemented various Titanium-based coatings [22-24], but several elements have been investigated as candidate substitute of Titanium component. Hafnium nitride (HfN) is one of the studied alternatives whereas its deposition, characterization and possible applications have been reported in literature over the last decade [25-30].

The literature presents that when processed as a thin films HfN hard coating has presented desirable properties for cutting tools such as: oxidation mitigation, high hardness in heat and better surface finish, which could generate a notorious improvement of the surface finish and increase of the useful life. Therefore, HfN-based coatings have been employed in ceramic and HSS cutting tools in machining of carbon steel workpieces [31-34]. Table 1 recompiles some reported mechanical properties between an uncoated HSS substrate and HfN sprayed coated HSS, which shows a significant hardness increase, which would increase tool lifetime during machining of metal part.

Table 1. Spray-coating HfN and High-Speed Steel mechanical properties [35-38].

Material	Elastic Module (GPa)	Hardness (GPa)	H/E	Melting point (°C)
High Speed Steel	190-210	7.336-8.179	0.034-0.043	4680
Spray-coating	225±10	12.8±1,6	0.06	4603

In this article an assessment was performed on the use of Hafnium Nitride (*HfN*) coatings, its durability and performance when deposited on a high-speed steel burin for aluminum roughing operations. Characterization techniques were used to identify less wear and a positive difference in the surface finish, as well as to increase the service life of the coated burin. The obtained test results indicate the effect of the coating in enhancing the quality of the surface finish of aluminum parts, suggesting that HfN coating can be potentially used onto cutting tools in manufacturing of mechanical components based on aluminum alloys.

2. METHODS AND MATERIALS

2.1. Coating deposition

Hafnium (Hf) target was used in a 4-inch diameter circular design with a purity of 99.99 %.

The ASSAB 17-burin substrates are cleaned in an ultrasound system, immersed in a sequence of ethanol and acetone for 15 minutes each cycle. Before deposition, the vacuum chamber was evacuated by the turbomolecular pump at a base pressure of 2.3x10-5 mbar in order to reduce the effects of the residual air. In the chamber, the substrates were subjected for 15 minutes to a bias voltage of -400 V (r.f.) with a power of 60 W (r.f.) in the argon plasma (Ar) to remove any oxide layer. On the substrates an intermediate layer of Hf was deposited, in order to increase the adhesion between the coatings and the substrate, this was done under continuous deposition for Hf at a r.f. power. 400 W, respectively, at an argon atmosphere for 5 minutes. The HfN deposition parameters were ratio N2/Ar = 20/80, in percentual form, the working pressure was 1.2*10-12 mbar, the polarization voltage was -30V, a temperature of 250 °C and a deposition time of 7.79 hours.

The equipment used is a system that consists of four four-inch diameter magnetron sputtering guns; three radio frequency sources (13.56 MHz), turbomolecular pumping system, high and low pressure gauges, pressure controllers; radiation heating system from room temperature up to 400 °C, digital flowmeters for four gases, wall-pass substrate holder with shaft to rotate the substrates, assisted by a speed-adjustable motor to create homogeneous thickness layers and grow in-situ layers of different materials.

Previous studies by Caicedo et al. detailed the employed deposition process, the characterization of physical-chemical and mechanical properties of this coating, including coating thickness, hardness, roughness, chemical composition, phases in the structure, adhesion with the substrate material, corrosion resistance, wear resistance, and microstructural examinations [33,39-41].

2.2. Cutting setup

For the cutting tests, the workpiece material was aluminum 6063-T5, with a diameter of 25.4 mm and a length of 100mm. A sheet metal was designed and assembled with the temperature optic sensor and the Printed Circuit Board (PCB) electronic modules. The system was mounted on a Leadwell CNC precision lathe, thus determining the temperature of the burin, the aluminum part, and the chip. The maximum temperature of each thermogram was plotted on a Graphical User Interface (GUI) and registered to be analyzed.

The standard cutting parameters for roughing with inserts are selected to be compared with the literature on sharp burins. The possible parameters were derived from the SANDVICK specifications and Kalpagian recommendations [9], considering the type of tool, cutting angles, and application. The cutting parameters where delimited, as shown in Table 2, establishing constant conditions for each test, making 12 runs per piece.

Table 2. Parameters of cutting test.

Cutting speed (m/min)	Cutting depth (mm)	Feed (mm/rev)	Workpiece diameter (mm)
217.5	1	0.65	28-16

The burins before coating and the tool as reference system (uncoated burin) were machined with a Jiansung Nantong Ching-Chuan universal tool grinding machine model 2M6420. The used angles are presented in Table 3, suggested by Kennametal for aluminum alloys.

Table 3. Conventional burin sharpness angles.

Attack on the rear	Attacking angle lateral	Frontal incident.	Side impact
20°	15°	12°	10°

2.3. Characterization conditions

The structure analysis of the films been done by X-Ray Diffraction (XRD), using a Panalytical X Pert PRO diffractometer with a radiation source of Cu kα (λ=1.5406 Å), employing the Bragg-Brentano configuration using a 2-Θ scanning from 30° to 60° scale. The morphological analysis and elemental composition were characterized by using Scanning Electron Microscopy - Energy dispersive spectroscopy (SEM-EDS). The power energy for the SEM bein of 20 kV, using a X 5,000 magnification with a 5μm scale, using a source SEIZZ scanning electron microscopy (SEM). The roughness and topography analyses of the films were studied using Atomic Force Microscopy (AFM), in contact mode trough AFM-Nanosurf

Easyscan 2 STM on an area of 55×55 μm. Mechanical analyses were performed via nano-indentations by using a Ubi1-HysitronTM device and a diamond Berkovich tip at variable loads. From these measurements, load–penetration depth curves of the coatings were obtained. Hardness and elastic modulus values were determined from the load–displacement curves. Errors were determined as the standard deviation from at least 10 different measurements in different points of the samples. A Nanovea, T2000 model tribometer was also used. The parameters implemented during the tests were speed and load. Using as a sliding pattern a ball made of 100Cr6 steel with a diameter of 6 mm, the applied load was 5 N with a total stroke length of 100 m.

After the test, the surface of the burins was characterized in its microstructure by SEIZZ scanning electron microscopy (SEM). The topographical characterization characterization of the wear surfaces is carried out using a Carl Zeiss Confocal Laser Scanning Microscope (LSCM) LSM 700 and the surface roughness of the samples has been measured on the average roughness *(Ra)* scale by a MD-E00RU02 Roughness Meter, using the 9230-ST-I-27 and the surface roughness observed an AFM analysis.

2.4. Temperature measurement system

The designed system (Fig. 1a) and its manufacture (Fig. 1b) allows the capture of a temperature matrix on a surface area. A modular and wireless electronic system was used together on a digital camera system containing the following components: thermal camera Adafruit AMG8833, a programmable microcontroller ESP-12E NodeMCU, a Bluetooth module HC05 V2, and Power-Bank 5v 1800 mAh.

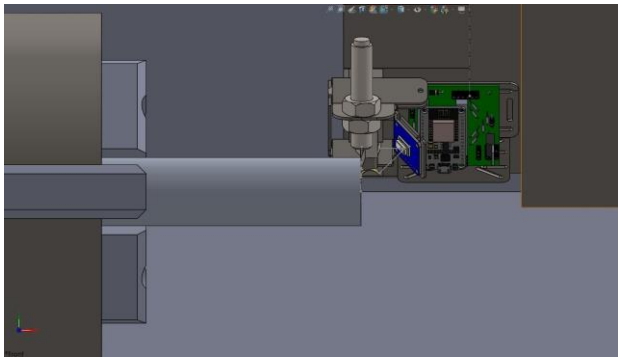

(a)

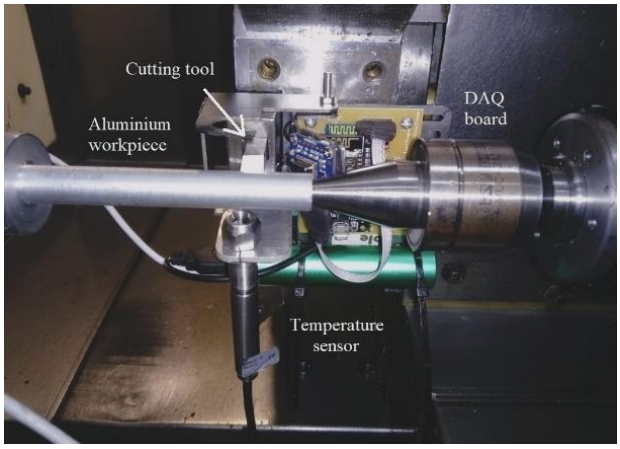

(b)

Fig. 1. Temperature measurement device.
(a) Computer-aided design of the set-up made with SolidWorks, (b) installed system in the CNC lathe.

Data is received wireless in a computer which graphs the temperature and the image captured by the thermal camera.

3. RESULTS

3.1. Coating characterization

Figure 2, the SEM micrograph has been used to determine the thickness that is 1.12 μm and proof of the interface and orientation of growth of the layer. In the cross-section images it is possible to observe the layer-substrate interface and the continuity of the layer throughout the cross section without severe cracks or deformations. The surface micrography exhibit a uniform layer with low imperfections (pores or micro cracks), supporting the low roughness of the layers obtained by AFM, which is sensitive to the intensity of secondary electrons emitted from the sample.

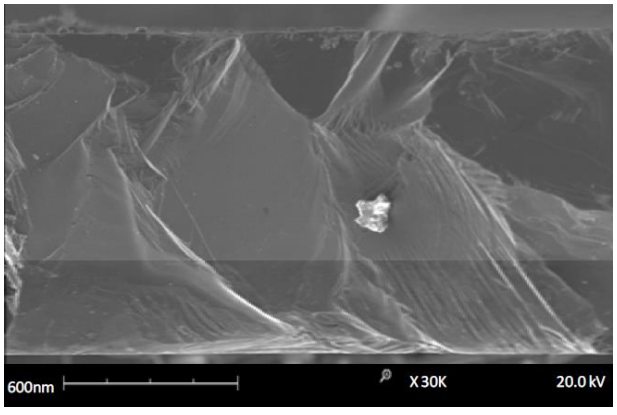

Fig. 2. SEM micrograph for the HfN layer.

X-ray diffraction (XRD) analyses indicate that the HfN layers under deposition conditions grew with a preferential orientation in the planes (111) and those of lower intensity were (200) and (220), the peak with plane (100), is related to Hf (Fig. 3) [32,39]. The experimental coating patterns represent the characteristic orientations of the powder samples according to the ICCD files JCPDF-00 033 0592. Of these patterns, simulated and experimental, is possible that the experimental pattern in HfN undergoes a short deviation in the values 2θ for the different intensities in relation to the simulated pattern, this difference is attributed to the misalignment of the lattice due to the tension and compression stress presented by the HfN layers, specifically to the negative polarization voltage applied to the substrate.

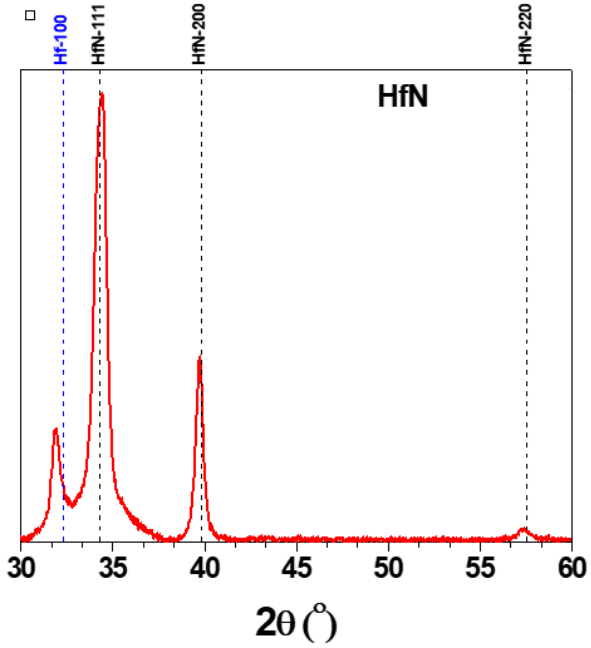

Fig. 3. XRD diffractogram of the HfN coating [32,39].

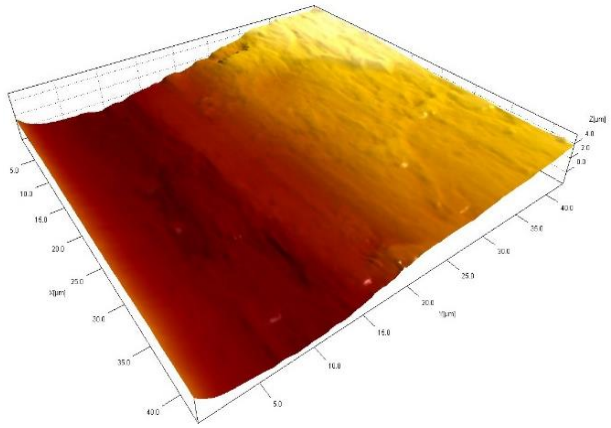

Fig. 4. AFM image of the HfN coating.

Figure 4 is the topography from which the average roughness (Ra) of the coating was obtained. Image Metrology's SPIP software was implemented, which found a roughness value for the coated tool, obtaining an *Ra* of 1091.58 nm, this value indicates surface finish which could generate an adequate behavior between the tool and the material by decreasing the friction in a tribological pair. According to the AFM analysis the obtained layers present very low grain sizes 61 ±2 nm and when the structure of these materials in the form of a thin layer gives rise to discontinuous grain boundaries that diminish the possibility of forming defects or pores.

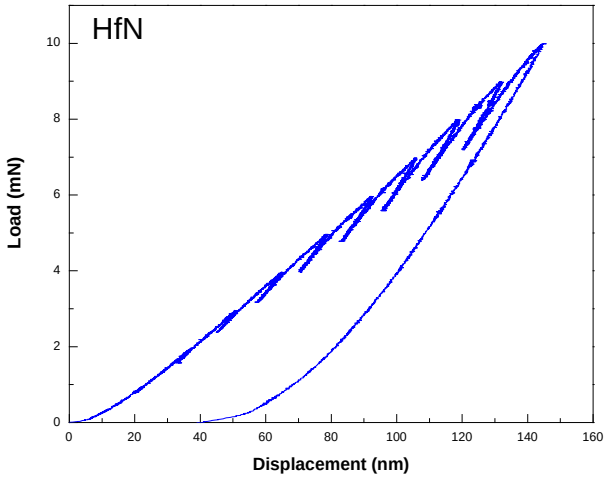

Fig. 5. Load-displacement curve for HfN coating.

Figure 5 indicates the loading and unloading curve obtained in the nanoindentation tests for the coatings, to calculate the values of hardness and elastic modulus were determined by Oliver and Pharr's method [42,43]. Hardness measurement is representative of the complete layer, due to the use of an indentation matrix with 16 points. It is important to emphasize that the hardness value obtained reaches the value of ~21 GPa. The dynamics of the mechanical behavior gives a consequent correlation with other properties such as Young's modulus, resistance to plastic deformation (H^3/E^2) and elastic recovery (R). Results obtained from the nanoindentation test are summarized in Table 4.

Table 4. Parameters resulting from the nano-indentation test.

H **(Gpa) ±0,1**	***Er*** **(GPa) ±3**	H^3/E^2	***R*** **(%)**
21	224	0.19	73

Regarding the above results, the literature reports [32,39] that the hardness of the interstitial nitrides of the transition metals varies depending on the crystalline orientation, with the orientation (111) generally being the hardest. Therefore, the mechanical behavior in the deposited layers may be associated with the higher proportion of crystallites in the HfN layer with a preferential orientation (111).

The coefficient of friction values generated with the HfN coated and the uncoated tribological burin pair and 100Cr6 steel ball are presented in Fig. 6. These curves show two different conditions. In the first range, the coefficient of friction, μ, begins at low levels, called the start-up period, and is associated with the mechanism of interfering friction due to the contact between the tips of the roughness of both counterparts, the steel ball and the surface. Increasing the sliding distance increases the coefficient of friction in the tribological pair, this due to the formation of wear particles generated by the rupture of the tips of the roughness. When the roughness of both surfaces are smoothed, the surface of the softer material, as it is in this study where the pin used is chrome steel, is moulded to the surface of the harder material, in this case the HfN films; thus reducing the coefficient of friction until the appearance of a stationary state. The second stage is called the steady-friction period and started after about 20m - 70m of sliding. In this station is generated a stabilization of the friction coefficient associated to the coexistence and opposition between the adhesive and interferential mechanisms. Fig. 6 reveal that the coated HSS has lower coefficient of friction.

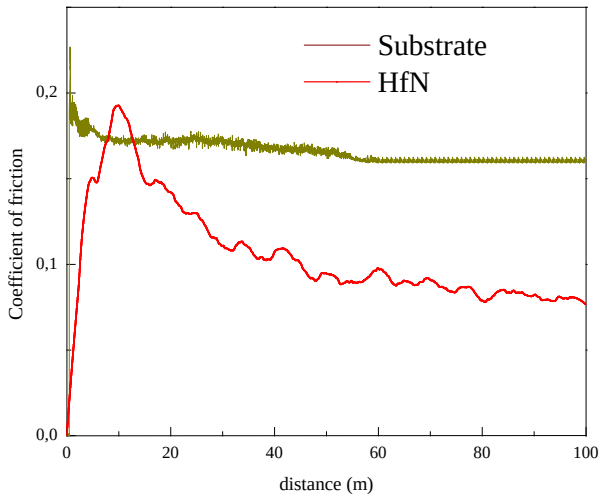

Fig. 6. Coefficient of friction of HfN thin film and substrate.

3.2. Tool wear

Micrographs of the burin edges are shown in the Fig. 7, where sharpness in the burin face (with and without coating), after 45 cycles is observed, no re-growth of the wear edge was observed. Nevertheless, in either system, a surface contact trace is observed due to the trace that the chip left during its displacement on the attack surface, leaving steel residues [44,45]. This contact trace is more visible in the uncoated burin, due to self-lubricant layer resulting from the HfN coating which improves its performance in wear processes, as previously reported [25-30,33,39-40]. Similarly, Fig. 8 shows the tool surface after 100 cutting cycles, showing built-up edge (BUE) formation and adhesive particles, revealing less adhesive track in the coated tool.

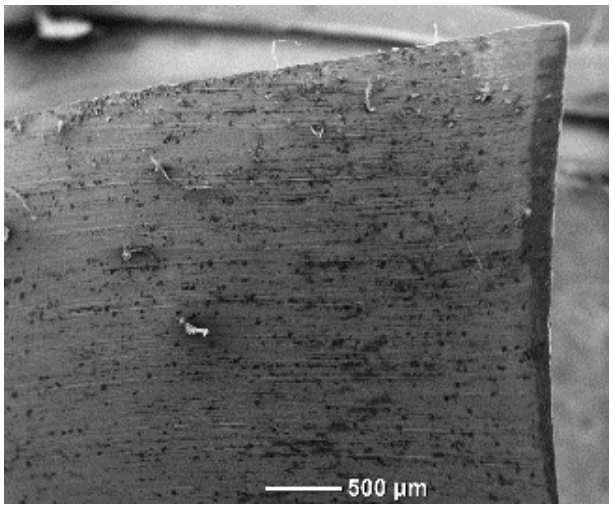

(a)

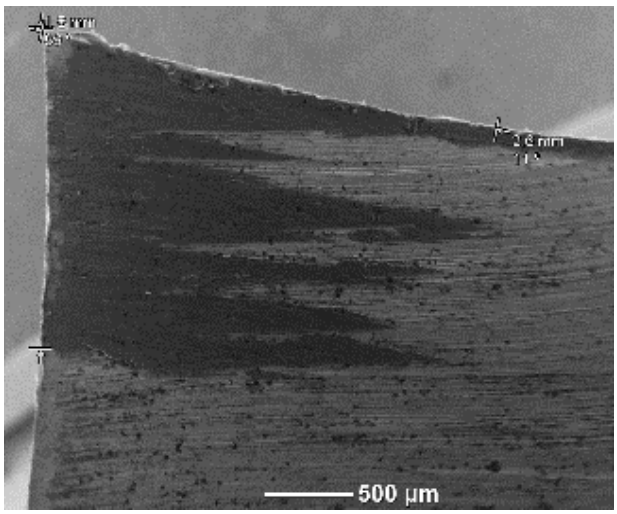

(b)

Fig. 7. SEM Micrographs. (a) uncoated burin and (b) the coated burin. A wear mark is observed after the 45 tests of material removal.

When the contact area of the tribological pair (tool-chip) is reduced, the cutting conditions vary as evidenced by the temperature system, where the temperature of the tool's leading edge indicates dissipation of the tool's energy to the chips removed, with an average temperature of 92 °C and 44 °C, for the uncoated and HfN-coated burins respectively, and an average variance of 0.012 °C and 0.0016 °C, detailed results can be consulted in [46]. A unified decrease in temperature, friction coefficient and workpiece surface roughness, indicates an enhancement of the tribological compatibility between the cutting tool and the machined workpiece [47].

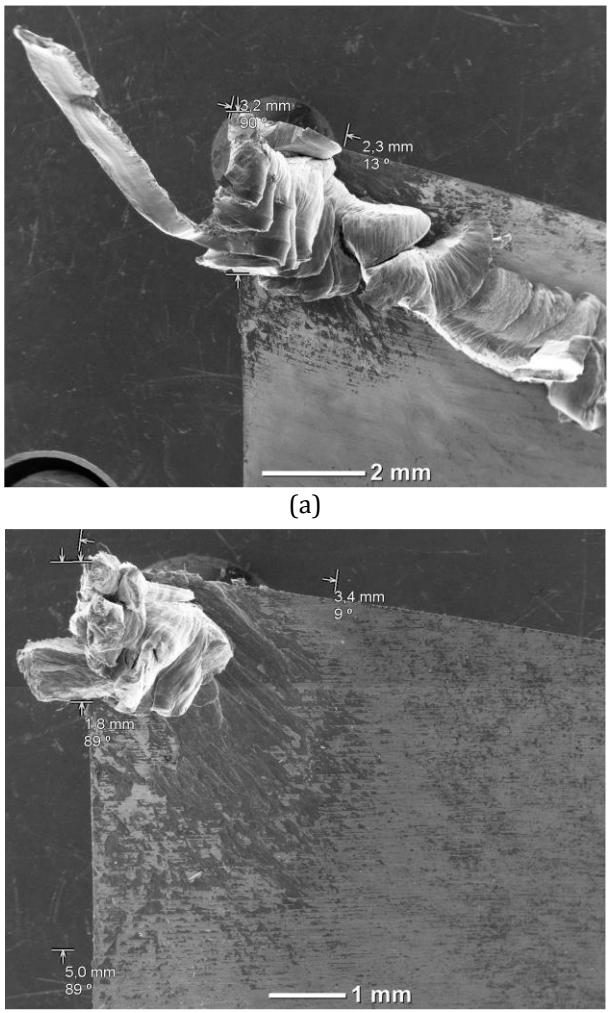

(a)

(b)

Fig. 8. SEM Micrographs after 100 cutting cycles (a) uncoated burin and (b) the coated burin. Adhered chip is observable for the both tools.

The re-growth edge on the incidence surface after 100 cutting cycles is shown in Fig. 9, using the EDS probe. Predominant wear mechanism strongly depends on various machining factors such as temperature increase, thermal cracks on the main edge, surface finishing, chip-to-tool contact area, and vibrations. Quantitative mapping of elements (Figs. 9b-9e) for the uncoated tool agree well with the tribological system [48].

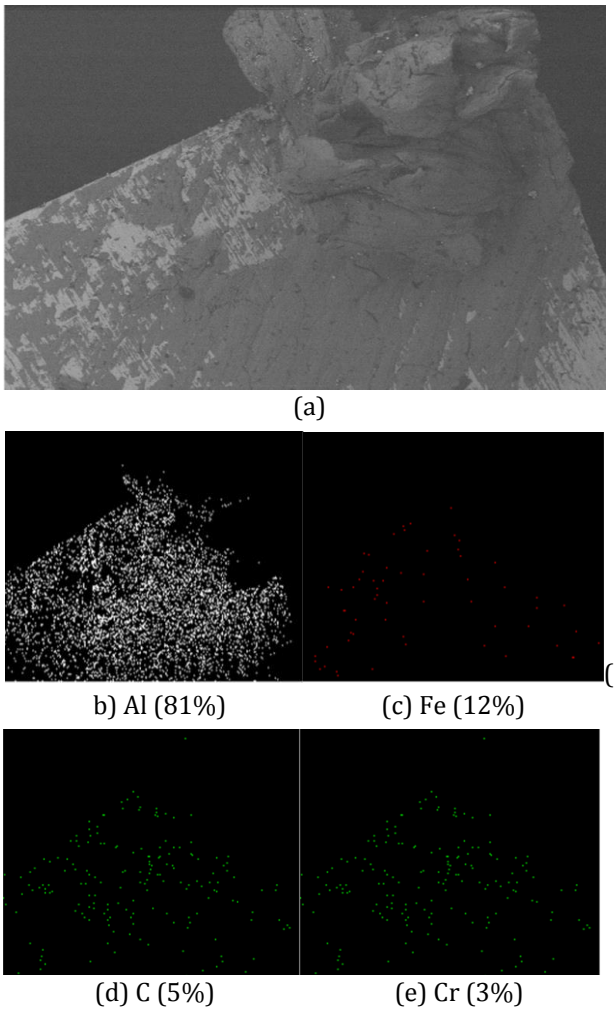

(a)

b) Al (81%) (c) Fe (12%)

(d) C (5%) (e) Cr (3%)

Fig. 9. SEM Micrograph corresponding to:
(*a*) uncoated and worn tool, (*b*) percentage of Aluminum bonded to the surface from the workpiece, (*c*) Iron corresponding to the protective element, (*d*) carbon related to the environment, (e) Chromium related to the buring.

The distribution of the chemical phases in the sample, indicates an amount close to 80 % of Al, and other elements such as Fe, Cr and C, with a lower percentage. Additionally, the microscopy image (Fig. 9a), where the morphology of the burin tip can be analyzed, shows a high chip contribution due to the friction generated between the surface of the roughing tool and the surface of the machined part (aluminum cylinder) thus, producing adhesion of the machined aluminum to the cutting edge. This

result suggest that the combination between the high cutting force, the friction in the tribological bur-steel pair and the contact temperature cause a catastrophic wear in the tip area, generating a premature reduction of the tool life, and generating a surface with an accumulated edge, which will negatively affect the surface finish of the part [49].

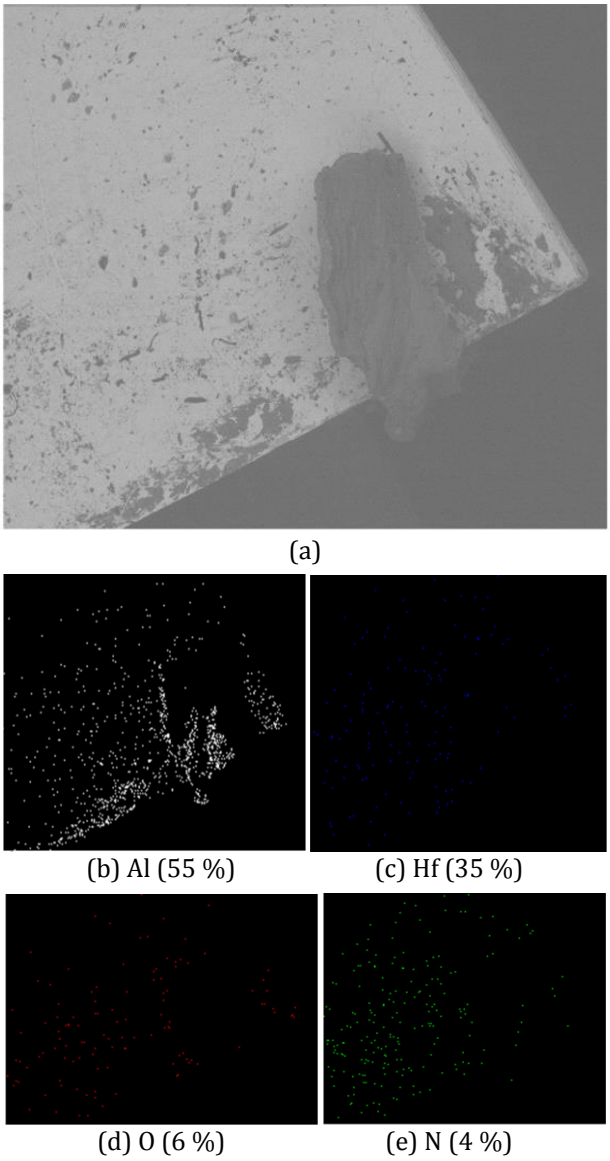

(a)

(b) Al (55 %) (c) Hf (35 %)

(d) O (6 %) (e) N (4 %)

Fig. 10. Micrograph corresponding to:
(*a*) coated and worn burin, (*b*) percentage of Aluminum bonded to the surface from the workpiece, (*c*) Hf corresponding to the protective element, (*d*) oxygen related to the environment, (*e*) nitrogen related to the coating.

The edge of the coated burin was analyzed using SEM to determine the effect of the HfN coating deposited on the burin. (Fig. 10a) micrograph clearly illustrates the wear generated at the edge and not at the tip thus suggesting that after machining process with total of 100 passes the tool life of the coated burin is not yet complete. Figure 10 indicates a decrease in the wear trace generated in comparison with the uncoated burin. Also, it can be determined that the HfN coatings showed a higher resistance to adhesive wear, due to the reduction of material adhered to the surface of the burin, where the lesser formation of chip accumulation decreases the variations in the quality of the cutting process and obtaining a better finish of the roughed part, which is also due to a decrease in the cutting temperature. Figs. 10b, 10c, 10d and 10e, show the percentages of the elements, where Al, Hf, O and N are found [50].

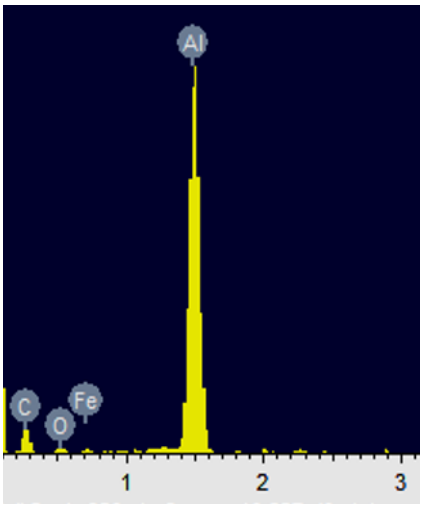

(a)

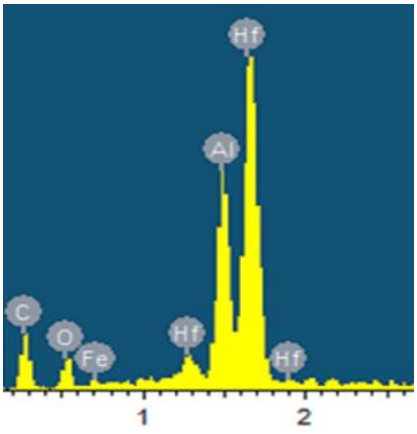

(b)

Fig. 11. EDX—spectrum of the worn surface of the (a) uncoated HSS tool, (b) HSS tool coated with HfN.

Figure 11 presents the EDX spectral of both worn tools and Table 5 unifies the chemical composition of worn surfaces. Indicating less adhesion of material from the aluminum workpiece and less worn material removed from the tool substrate.

Table 5. Chemical composition of worn surfaces.

Element	*Uncoated tool*		*HfN coated tool*	
	Weight%	Atomic%	Weight%	Atomic%
C K	52.55	69.33	29.15	65.24
O K	7.23	7.16	10.09	16.96
Al K	39.83	23.39	9.29	9.26
Fe K	0.39	0.11	2.4	1.15
Hf L	-	-	49.07	7.39
Totals	100		100	

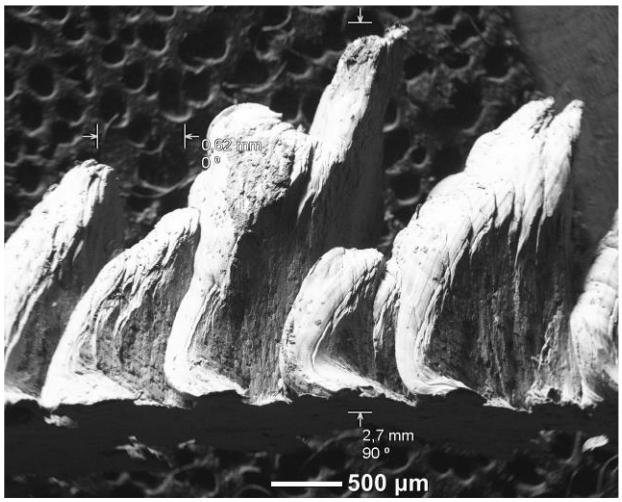

(a)

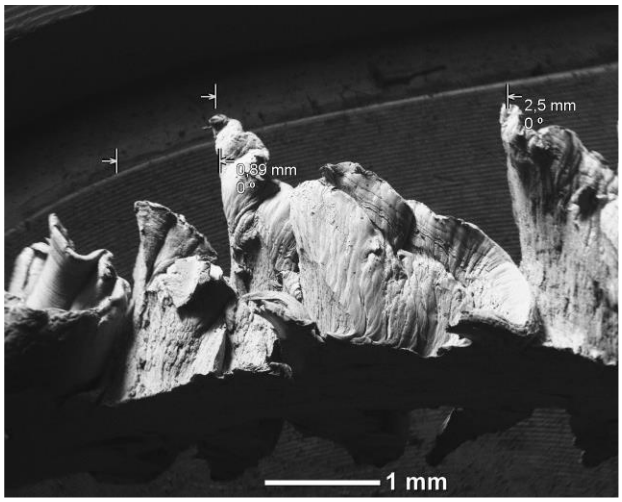

(b)

Fig. 12. SEM micrograph of obtained chips with (a) uncoated HSS tool, (b) HSS tool coated with HfN.

In both tests the chip flowed continuously as shown in Fig. 12, but for the uncoated burin the angle of chip formation suggested an abrasion process. Additionally, there were some interruptions between the cycles because some deburring, which had to be removed to continue with the adequate process. In the case of the HfN burin, less material accumulation was generated, which is associated with adhesive-type wear, and thus less wear in comparison with other uncoated tribological systems. Additionally, this could generate a low roughness which is caused by a lower coefficient of friction [47], as obtained in the results of the below section.

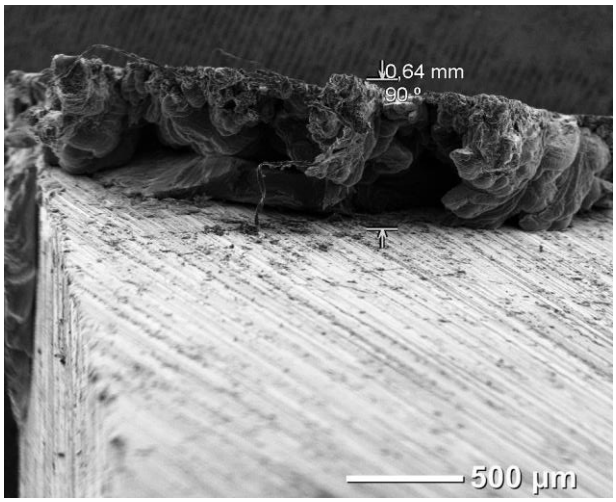

(a)

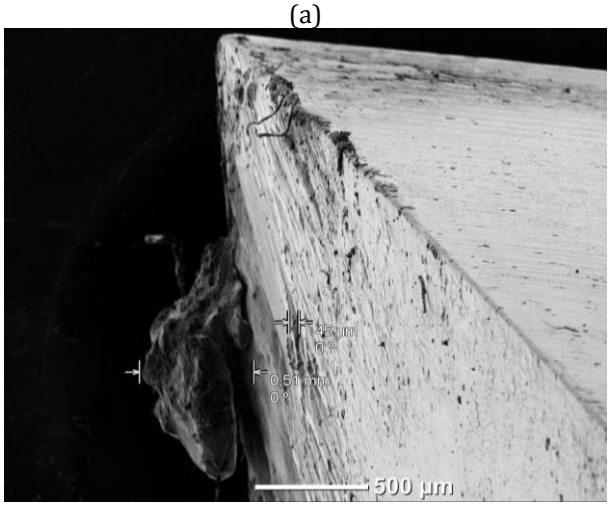

(b)

Fig. 13. SEM micrographs. (*a*) Uncoated burin with re-growth and (*b*) coated burin with re-growth.

Figure 13a indicates the uncoated burin after 100 cycles, generating an increase of 0.64 mm on the cutting edge and the upper and lateral edges. This adhesion of material to the tool acts as an obstacle on the cutting edge, increasing the friction of the tribological system and consequently the surface roughness of the machined part, along with the possible formation of other surface imperfections. In the case of the coated burin, Fig. 13b, only chip adhesion on the side is obtained, 0.54 mm, indicating that the use of coated burins, the wear is lower with the cutting parameters recommended by the manufacturers [51].

3.3. Workpiece roughness

The analysis of the final surface after 100 passes was the evaluation of the average roughness (*Ra*) performed by Laser Scanning Confocal Microscope. The equipment avoids physical contact with the part to be measured, allowing topographic measurement (shape and roughness in 3D) with speed and scan resolution higher than those offered by the roughness meter. It was determined that the obtained value is not affected by the variation of neither the parameters of lateral resolution nor the vertical resolution, since the range of variation of these resolutions is smaller to the topographic details in study.

Figure 14 illustrates the surface topography obtained with both types of burins. When comparing the machined areas, Fig. 14 (a - d), uniformity was observed grater in the machined part with the coated burin and lower aluminum roughness. This result is due to the changes in chip formation, and energy dissipation during the cutting process.

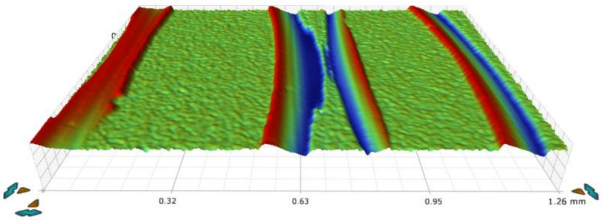

(a)

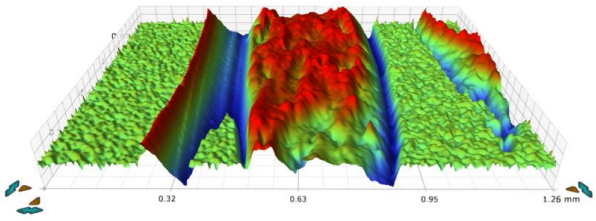

(b)

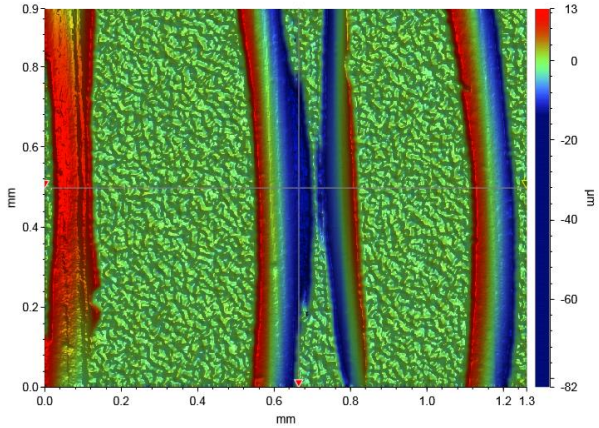

(c) Ra = 1.23 µm

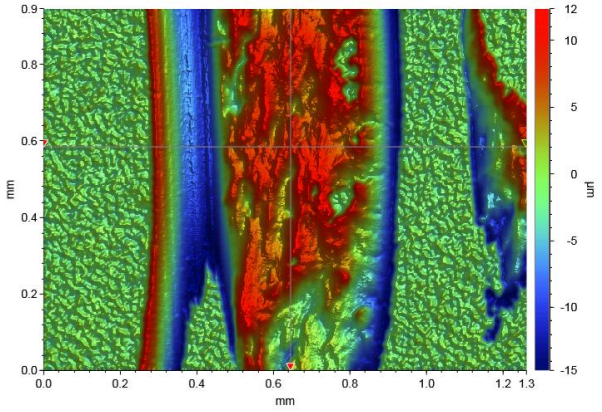

(d) Ra = 5.32 µm

Fig. 14. Laser Scanning Confocal Microscope view of aluminum machined part with *(a)* coated tool *(b)* uncoated tool, *(c)* 2-D surface, of the roughed surface with the coated tool where the roughness value *Ra* is indicated, *(d)* 2-D surface, of the roughed surface without coating, the roughness value *Ra* is indicated.

While the coated burin reduces friction in the system and lower tool temperature, the combined results suggest that the cutting energy is dissipated across the machined surface, which affects the plastic deformation of the aluminum and generates less surface irregularities in the machined part. In this regard these results strongly suggest the coated burin also as a surface finish enhancer.

4. CONCLUSION

Using HfN monolayer as hard coating for cutting tools in Aluminum turning improves the resistance to wear by reducing the temperature generated during cutting, the adhesion of material, and less friction with abrasive particles. For machining of aluminum parts, the variation of the tribological process generated by the properties of HfN in the energy diffusion, modifies the chip release and the tool-workpiece contact. Consequently, the use of HfN protects the tool from adhesive and abrasive wear mechanisms in roughing. The optimum materials and cutting conditions for HfN coatings must be identified for machining processes using in further studies, along with performance comparison with the other coating.

Acknowledgement

This research was supported by "*Vicerectoria de investigaciones Universidad Militar Nueva Granada*" under contract ING 3123 validity 2020-2021.

REFERENCE

[1] A. Inspektor, P.A. Salvador, *Architecture of PVD coatings for metalcutting applications: A review*, Surface and Coatings Technology, vol. 257, pp. 138-153, 2014, doi: 10.1016/j.surfcoat.2014.08.068

[2] V. Sousa, F. Silva, *Recent Advances in Turning Processes Using Coated Tools—A Comprehensive Review*, Metals, vol. 10, iss. 2, pp. 170-180, 2020, doi: 10.3390/met10020170

[3] Y. Chen, J. Wang, M. Chen, *Enhancing the machining performance by cutting tool surface modifications: a focused review*, Machining Science and Technology, vol. 23, iss. 3, pp. 477-509, 2019, doi: 10.1080/10910344.2019.1575412

[4] E.A. Jr. Starke, H.M.M.A. Rashed, *Alloys: Aluminum*, Reference Module in Materials Science and Materials Engineering, 2017, doi: 10.1016/B978-0-12-803581-8.09210-9

[5] M.C. Jr. Santos, A.R. Machado, W.F. Sales, M.A.S. Barrozo, E.O. Ezugwu, *Machining of aluminum alloys: a review*, The International Journal of Advanced Manufacturing Technology, vol. 86, pp. 3067–3080, 2016, doi: 10.1007/s00170-016-8431-9

[6] I. Boromei, L. Ceschini, C. Martini, R. Sola, *Aluminium bronze-steel sliding contact in packaging applications: Failure analysis and lab-scale tribological tests*, Engineering Failure Analysis, vol. 112, pp. 104528, 2020, doi: 10.1016/j.engfailanal.2020.104528

[7] S. Sardar, S.K. Karmakar, D. Das, *High stress abrasive wear characteristics of Al 7075 alloy and 7075/Al2O3 composite*, Measurement, vol. 127, pp. 42-62, 2018, doi: 10.1016/j.measurement.2018.05.090

[8] L.-l. Wang, W. Wang, Y.-l. Fan, X.-x. Qi, J.-h. Liu, Z..y. Zhang, *Effects of Al and Ni doping on oxidation and corrosion resistance of electrophoretic deposited YSZ coatings*, Transactions of Nonferrous Metals Society of China, vol. 27, iss. 7, pp. 1551-1557, 2017, doi: 10.1016/S1003-6326(17)60176-6

[9] S. Kalpakjian, S.R. Schmid, *Machining processes: turning and hole making*. Manufacturing engineering and technology, 7th ed, Prentice Hall, pp. 625–667, 2014.

[10] S. Kalpakjian, S.R. Schmid, *Surface roughness and measurement; friction, wear and lubrication*. Manufacturing engineering and technology, 7th ed, Prentice Hall, pp. 963–984, 2014.

[11] S. Kalpakjian, S.R. Schmid, *Quality assurance, testing, and inspection*. Manufacturing engineering and technology, 7th ed, Prentice Hall, pp. 1030–1056, 2014.

[12] C. Moganapriya, M. Vigneshwaran, G. Abbas, A. Ragavendran, V.C. Harissh Ragavendra, R. Rajasekar, *Technical performance of nano-layered CNC cutting tool inserts – An extensive review*, MaterialsToday: Proceedings, In Press, 2020, doi: 10.1016/j.matpr.2020.02.731

[13] J. Yuan, J. Dosbaeva, D. Covelli, J. Boyd, G.S. Fox-Rabinovich, S.C. Veldhuis, *Study of Tribofilms Generation at Different Cutting Speeds in Dry Machining Hardened AISI T1 and AISI D2 Steel*, Proceedings of the Institution of Mechanical Engineers, Part J: Journal of Engineering Tribology, vol. 232, iss. 7, pp. 910–918, 2018, doi: 10.1177/1350650117733921

[14] T.L. Brzezinka, J. Rao, M. Chowdhury, J. Kohlscheen, G.S.F. Rabinovich, S.C. Veldhuis, J.L. Endrino *Hybrid Ti-MoS2 Coatings for Dry Machining of Aluminium Alloys*, Coatings, vol. 7, iss. 9, p. 149, 2017, doi: 10.3390/coatings7090149

[15] V.F.C. Sousa, F.J.G. Silva, *Recent Advances on Coated Milling Tool Technology—A Comprehensive Review*, Coatings, vol. 10, iss. 3, p. 235, 2020, doi: 10.3390/coatings10030235

[16] J. Zhao, Z. Liu, B. Wang, J. Hu, Y. Wan, *Tool coating effects on cutting temperature during metal cutting processes: Comprehensive review and future research directions*, Mechanical Systems and Signal Processing, vol. 150, p. 107302, 2021, doi: 10.1016/j.ymssp.2020.107302

[17] G. Skordaris, K.-D. Bouzakis, T. Kotsanis, P. Charalampous, *A Critical Review of Measures for an Effective Application of Nano-Structured Coatings in Milling*, Tribology in Industry, vol. 39, no. 2, pp. 211-218, 2017, doi: 10.24874/ti.2017.39.02.08

[18] M. Sokovic, J. Kopac, L.A. Dobrzanski, J. Mikula, K. Golombek, D. Pakula, *Cutting Characteristics of PVD and CVD - Coated Ceramic Tool Inserts,* Tribology in Industry, vol. 28, no. 1, pp. 3-8, 2006.

[19] Z. Yin, S. Yan, J. Ye, Z. Zhu, J. Yuan, *Cutting performance of microwave-sintered sub-crystal Al2O3/SiC ceramic tool in dry cutting of hardened steel*, Ceramics International, vol. 45, iss. 13, pp. 16113-16120, 2019, doi: 10.1016/j.ceramint.2019.05.128

[20] T.A. Otitoju, P.U. Okoye, G. Chen, Y. Li, M.O. Okoye, S. Li, *Advanced ceramic components: Materials, fabrication, and applications*, Journal of Industrial and Engineering Chemistry, vol. 85, pp. 34-65, 2020, doi: 10.1016/j.jiec.2020.02.002

[21] F. Molaiekiya, M. Aramesh, S.C. Veldhuis, *Chip formation and tribological behavior in high-speed milling of IN718 with ceramic tools*, Wear, vol. 446–447, pp, 203191, 2020, doi: 10.1016/j.wear.2020.203191

[22] A.A. Vereschaka, S.N. Grigoriev, N.N. Sitnikov, G.V. Oganyan, A. Batako, *Working efficiency of cutting tools with multilayer nano-structured Ti-TiCN-(Ti,Al)CN and Ti-TiCN-(Ti,Al,Cr)CN coatings: Analysis of cutting properties, wear mechanism and diffusion processes,* Surface and Coatings Technology, vol. 332, pp. 198–213, 2017, doi: 10.1016/j.surfcoat.2017.10.027

[23] K.D. Bouzakis, N. Michailidis, G. Skordaris, E. Bouzakis, D. Biermann, R. M'Saoubi, *Cutting with coated tools: coating technologies, characterization methods and performance optimization,* CIRP Annals, vol. 61, iss. 2, pp. 703–723, 2012, doi: 10.1016/j.cirp.2012.05.006

[24] M. Tkadletz, N. Schalk, R. Daniel, J. Keckes, C. Czettl, C. Mitterer. *Advanced characterization methods for wear resistant hard coatings: a review on recent progress.* Surface and Coatings Technology, vol. 285, pp. 31-46, 2016, doi: 10.1016/j.surfcoat.2015.11.016

[25] W. Tillmann, N.F. Lopes Dias, D. Stangier, *Effect of Hf on the microstructure, mechanical properties, and oxidation behavior of sputtered CrAlN films,* Vacuum, vol. 154, pp. 208–213, 2018, doi: 10.1016/j.vacuum.2018.05.015

[26] W. Tillmann, N.F. Lopes Dias, D. Stangier, M. Tolan, M. Paulus, *Structure and mechanical properties of hafnium nitride films deposited by direct current, mid-frequency, and high-power impulse magnetron sputtering*, Thin Solid Films, vol. 669, pp. 65–71, doi: 10.1016/j.tsf.2018.10.035

[27] F. Guo, J. Wang, Y. Du, J. Wang, S.-L. Shang, S. Li, L. Chen, *First-principles study of adsorption and diffusion of oxygen on surfaces of TiN, ZrN and HfN*, Applied Surface Science, vol. 452, pp. 457–462, 2018, doi: 10.1016/j.apsusc.2018.05.052

[28] W.F. Piedrahita, W. Aperador, J.C. Caicedo, P. Prieto, *Evolution of physical properties in hafnium carbonitride thin films*, Journal of Alloys and Compounds, vol. 690, pp. 485–496, 2017, doi: 10.1016/j.jallcom.2016.08.109

[29] J. Song, L. Cao, L. Jiang, G. Liang, J. Gao, D. Li, S. Wang, M. Lv, *Effect of HfN, HfC and HfB2 additives on phase transformation, microstructure and mechanical properties of ZrO2-based ceramics,* Ceramics International, vol. 44, iss. 5, pp. 5371–5377, 2018, doi: 10.1016/j.ceramint.2017.12.164

[30] W. Piedrahita, J.C. Caicedo, W. Aperador, *Tribological and Electrochemical Properties of AISI D3 Steel Coated with Hafnium Carbon Nitride*, Tribology in Industry, vol. 40, no. 3, pp. 488-500, 2018, doi: 10.24874/ti.2018.40.03.14

[31] P.A.G. Duran, J.H. Navarro-Devia, W.A. Chaparro, *Machining With Cutting Tool Coated With Monolayer Of HfN*, Tecciencia, vol. 11, no. 21, pp 1-6, 2016, doi: 10.18180/tecciencia.2016.21.1

[32] J.H. Navarro-Devia, W.A. Aperador, A. Delgado, *Evaluación del Desempeño de Buriles con Recubrimiento Monocapas de Nitruro de Hafnio en el Proceso de Mecanizado // Performance Evaluation of Monolayer Hafnium Nitride Coated Tool for Cutting*, Información Tecnológica, vol. 27, no. 1, 2016, doi: 10.4067/S0718-07642016000100014

[33] C. Escobar, H.H. Caicedo, J.C. Caicedo, *Hafnium and vanadium nitride heterostrutures applied to machining devices*, The International Journal of Advanced Manufacturing Technology, vol. 82 pp. 369–378, 2016, doi: 10.1007/s00170-015-7345-2

[34] J.H. Navarro Devia, W.A. Chaparro, J.C. Lizarazo, *Evaluation of Single Layer Hafnium Nitride Coated Tool for Metal Cutting*, MRS Online Proceedings Library (OPL), vol. 1815, 2016, doi: 10.1557/opl.2016.91

[35] American Elements - Hafnium Nitride, at: www.americanelements.com/hafnium-nitride-25817-87-2, accessed: 29.06.2020.

[36] AZoM, "*M2 Molybdenum High Speed Tool Steel (UNS T11302)*" 2012 at: www.azom.com/article.aspx?ArticleID=6174, accessed: 19.07.2020.

[37] BÖHLER S630 High Speed Steel, Kapfenberg, p. 17, 2015, at: www.bohler-edelstahl.com/app/uploads/sites/92/2019/09/S630En.pdf, accessed: 19.07.2020.

[38] Y. Chen, T. Laha, K. Balani, A. Agarwal, *Nanomechanical properties of hafnium nitride coating*, *Scripta Materialia*, vol. 58, iss. 12, pp. 1121–1124, 2008, doi: 10.1016/j.scriptamat.2008.02.012

[39] C.A. Escobar, J.C. Caicedo, W. Aperador, *Corrosion resistant surface for vanadium nitride and hafnium nitride layers as function of grain size*, Journal of Physics and Chemistry of Solids, vol. 75, iss. 1, pp. 23–30, 2014, doi: 10.1016/j.jpcs.2013.07.024

[40] C. Escobar, M. Villarreal, J. C. Caicedo, J. Esteve, P. Prieto, *Mechanical and tribological behavior of VN and HfN films deposited via reactive magnetron sputtering*, Surface Review and Letters, vol. 20, no. 3n4, p. 1350040, 2013, doi: 10.1142/S0218625X13500406

[41] C. Escobar, J.C. Caicedo, W. Aperador, A. Delgado, P. Prieto, *Improve on Corrosion Resistant Surface for AISI 4140 Steel Coated with VN and HfN Single Layer Films*, International Journal of Electrochemical Science, vol. 8, pp. 7591–7607, 2013.

[42] W.C. Oliver, G.M. Pharr, *An improved technique for determining hardness and elastic modulus using load and displacement sensing indentation experiments*, Journal of Materials Research, vol. 7, iss. 6, pp. 1564–1583, 1992, doi: 10.1557/JMR.1992.1564

[43] S.P. Baker, J. Liu, *Nanoindentation techniques*, Reference module in materials science and materials engineering, 2016, doi: 10.1016/B978-0-12-803581-8.02586-8

[44] S. Baron, D. Desmond, E. Ahearne, *The fundamental mechanisms of wear of cemented carbide in continuous cutting of medical grade cobalt chromium alloy (ASTM F75)*, Wear, vol. 424–425, pp. 89-96, 2019, doi: 10.1016/j.wear.2019.01.096

[45] J. Xu, M. El Mansori, J. Voisin, M. Chen, F. Ren, *On the interpretation of drilling CFRP/Ti6Al4V stacks using the orthogonal cutting method: Chip removal mode and subsurface damage formation*, Journal of Manufacturing Processes, vol. 44, pp. 435-447, 2019, doi: 10.1016/j.jmapro.2019.05.052

[46] J. Ortiz, *HSS Turning tool life study coated with Hafnium Nitride [Hf-N] during aluminum machining*, Bachelor thesis, Universidad Militar Nueva Granada, Colombia, 2020, at: http://hdl.handle.net/10654/32591

[47] J.H. Navarro-Devia, C. Amaya, J.C. Caicedo, J.H. Martínez, W. Aperador, *Hafnium and vanadium nitride multilayer coatings [HfN/VN]n deposited onto HSS cutting tools for dry turning of a low carbon steel: a tribological compatibility case study*, The International Journal of Advanced Manufacturing Technology, vol. 101, pp. 2065–2081, 2019, doi: 10.1007/s00170-018-3020-8

[48] A. Gregorio, T. Santos, R. Rossi, A.M.P. Jesus, J.C. Outeiro, P.A.R. Rosa, *Tribology of metal cutting: newly formed underside of chip*, Procedia CIRP, vol. 82, pp. 136-141, 2019, doi: 10.1016/j.procir.2019.04.034

[49] B. Guimarães, C.M. Fernandes, D. Figueiredo, M.F. Cerqueira, O. Carvalho, F.S. Silva, G. Miranda, *A novel approach to reduce in-service temperature in WC-Co cutting tools*, Ceramics International, vol. 46, iss. 3, pp. 3002-3008, 2020, doi: 10.1016/j.ceramint.2019.09.299

[50] Z. Fang, T. Obikawa, *Influence of cutting fluid flow on tool wear in high-pressure coolant turning using a novel internally cooled insert*, Journal of Manufacturing Processes, vol. 56, part A, pp. 1114-1125, 2020, doi: 10.1016/j.jmapro.2020.05.028

[51] S. Ghorbani, V.V. Kopilov, N.I. Polushin, V.A. Rogov, *Experimental and analytical research on relationship between tool life and vibration in cutting process*, Archives of Civil and Mechanical Engineering, vol. 18, iss. 3, pp. 844-862, 2018, doi: 10.1016/j.acme.2018.01.007